



DIAGNOSIS OF CENTRIFUGAL PUMP SPEED FLUCTUATION BY USING VORTEX DYNAMICS

L. Cheng^a, Y. L. Zhang^{a,†}, J. F. Li^b

^a College of Mechanical Engineering & Key Laboratory of Air-driven Equipment Technology of Zhejiang Province, Quzhou University, Quzhou, Zhejiang, 324000, China

^b College of Mechanical Engineering, Zhejiang University of Technology, Hangzhou, Zhejiang, 310023, China

ABSTRACT

The internal characteristics during rotational speed fluctuation have an important influence on centrifugal pump to avoid or utilize its transient performance. In this paper, a circulation piping system that includes a low-specific-speed centrifugal pump is established to study the energy distribution characteristics in a centrifugal pump during speed fluctuation. The unsteady flow in the entire system is numerically calculated with a user-defined function, the sliding grid method, and the RNG $k-\varepsilon$ turbulence model. Then, the energy distribution of the transient flow field in the centrifugal pump model during speed fluctuation is diagnosed with vortex dynamics by using flow section and boundary vorticity flow diagnosis methods. Results confirm that the total pressure flow energy is relatively high in the process of speed reduction because of the small hydraulic loss, and the opposite was observed in the process of speed increase. The change laws of instantaneous dimensionless head and instantaneous dimensionless flow during speed fluctuation are contrary to that of speed fluctuation. This study provides a reference for the investigation of energy distribution characteristics in the process of speed fluctuation.

Keywords: Pump; Rotational speed; Fluctuation; Vortex dynamics; BVF

1. INTRODUCTION

Pump products are widely used to deliver all kinds of fluid medium in petrochemical engineering, sea water desalination, and farmland drainage and irrigation, etc., which are commonly used only under stable working conditions, but unstable working conditions, such as startup, shutdown, flow adjustment during operation, and speed fluctuation, arise inevitably. Extant research on the performance of pump products has focused on stable conditions, and performance research under unstable conditions has concentrated on startup (Tsukamoto and Ohashi (1982), Dazin *et al.* (2007), Duplaa *et al.* (2010), Li *et al.* (2010), Tanaka and Tsukamoto (1999), Lefebvre and Barker (1995)), shutdown (Tanaka and Tsukamoto (1999), Lefebvre and Barker (1995), Tsukamoto *et al.* (1986), Wu *et al.* (2014), Liu *et al.* (2011), Zhang *et al.* (2019)), and flow adjustment during operation (Tanaka and Tsukamoto (1999), Wu *et al.* (2010)). Only a few studies have been conducted on internal and external transient characteristics in the process of speed fluctuation.

The speed fluctuation of centrifugal pumps is an unsteady flow process with positive and negative flow accelerations in the acceleration and deceleration phases respectively, and the kinetic and pressure energy of the medium are converted intensely. A few studies on the speed fluctuation process have been conducted in the world. For example, the Japanese scholar Tsukamoto *et al.* used the singularity method to conduct experimental measurements and theoretical analyses of the transient characteristics of a low-specific-speed centrifugal pump with sinusoidal speed (Tsukamoto *et al.* (1995)). He discovered that the higher the speed fluctuation frequency is, the more obvious the performance difference is between transient and quasi-steady states. The author also proposed a precondition for the application of the

quasi-steady-state hypothesis on the basis of his own research conditions. This study is one of the few that investigated real-time fluctuations in pump speed.

The previous study applied the computational fluid dynamics (CFD) method to the numerical calculation of a circulating pipeline system that includes a centrifugal pump with a low specific speed to investigate the transient response characteristics of the flow when the rotating speed of the centrifugal pump fluctuates (Zhang *et al.* (2014)). In the simulation, the pump inlet and outlet were solved by self-coupling without boundary conditions. The results showed that compared with the characteristics of speed fluctuation, those of the flow response lagged slightly, and the head was highly responsive to speed fluctuation. The response fluctuation laws of inlet and outlet static pressure were contradictory, but the response law of dynamic pressure was nearly unchanged. The dimensionless head and dimensionless flow presented similar changing rules, which were nearly opposite those of speed variation. In general, the vortex distribution area in the quasi-steady-state calculation was extensive, and the quasi-steady-state assumption could not be used to predict transient behavior. The other behavior is also found in other flow (Gu *et al.* (2020), Abed *et al.* (2020), Xue *et al.* (2022), Dai *et al.* (2021)).

To analyze further the transient flow structure and the rationality of the energy distribution in the pump during the speed fluctuation process and its influence on transient characteristics, this study used the vortex dynamics method to determine the transient flow field distribution in the process of speed fluctuation on the basis of the numerical simulation results of the centrifugal pump speed fluctuation process obtained via CFD technology in the early stage. The total pressure flow distribution and axial component distribution of the boundary vorticity flow were used to characterize the fluid energy change and effect of the impeller on fluid work. The value of the total

[†] Corresponding author. Email: zhang002@sina.com

pressure flow in the cross section was used to analyze the conversion of the impeller's mechanical and fluid energy.

This paper presents an unsteady analysis and diagnosis of the internal flow field evolution of centrifugal pump speed fluctuation by using the vortex dynamics method. The diagnosis method and results are provided, and the results are analyzed to establish a basis for a special unsteady flow field analysis and engineering optimization of pump speed fluctuation.

2. PHYSICAL MODEL AND METHOD

2.1 Physical model

The centrifugal pump model adopted in this study is completely consistent with that used in literature (Zhao and Zhang (2016)), and its rated parameters are as follows: the flow is 6 m³/h, the head is 8 m, and the speed is 1450 r/min. The established circulation pipeline system, which is also completely consistent with that in literature (Zhao and Zhang (2016)), is shown in Figure 1(a). GAMBIT software was used for meshing, and the result of centrifugal pump meshing is shown in Figure 1(b). An unstructured tetrahedral mesh was adopted for the impeller and volute area, and a structured hexahedral mesh was used for the other calculation domains. A grid correlation check indicated that when the change in the calculation head was less than 2%, the requirement of grid independence is met. The final total number of grids was set to 641,902 in consideration of computational efficiency. The number of grids in the impeller, volute, and piping system areas was 280,772, 191,177, and 169,953, respectively. The number of grids was still insufficient for simulating the flow in the boundary layer, but it was sufficient for predicting external characteristics. Grid quality inspection showed that the equal angle slope and equal size slope of the grid were not more than 0.83; hence, the grid quality was good.

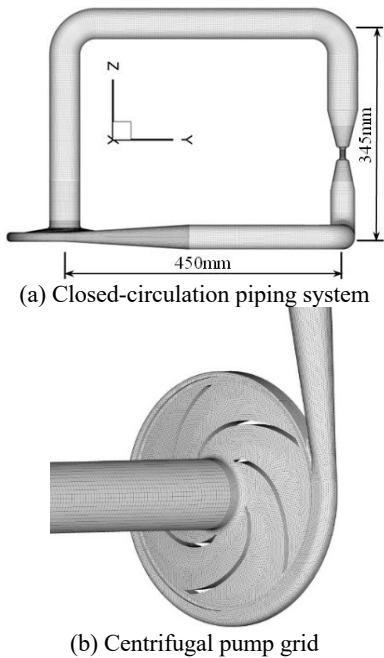


Fig. 1 Computational domain and grid

2.2 Computational method

The speed fluctuation of the centrifugal pump model changed in accordance with the sinusoidal law, as shown below (r/min). In accordance with the secondary development interface provided by FLUENT software, the speed change rule was loaded by writing a user-defined function.

$$n = 1450 + 500\sin(20\pi t) \quad (1)$$

The speed fluctuation situation is shown in Figure 2. The relative fluctuation range reached 34.5%, and the speed was in a state of severe fluctuation. The vortex dynamics diagnosis problem was discussed based on the unsteady flow field results of the previous speed fluctuation process.

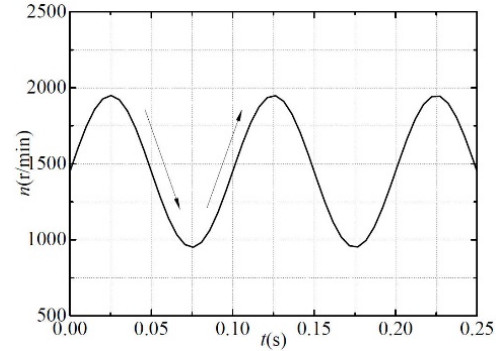


Fig. 2 Speed fluctuation situation

The unsteady turbulence calculation in this study used the RNG $k-\epsilon$ two-equation model to close the Reynolds average equation (Yakhot and Orzag (1986)). This turbulence model considers the rotation and swirl flow conditions in average flow and can effectively handle flows with high strain rates and large streamline curvatures.

$$\begin{cases} \rho \frac{dk}{dt} = \frac{\partial}{\partial x_j} \left(\alpha_k \mu_{\text{eff}} \frac{\partial k}{\partial x_j} \right) + 2\mu_i \overline{S}_{ij} \frac{\partial \bar{u}_i}{\partial x_j} - \rho \epsilon \\ \rho \frac{d\epsilon}{dt} = \frac{\partial}{\partial x_j} \left(\alpha_\epsilon \mu_{\text{eff}} \frac{\partial \epsilon}{\partial x_j} \right) + 2C_{1\epsilon} \frac{\epsilon}{k} \overline{v}_i \overline{S}_{ij} \frac{\partial \bar{u}_i}{\partial x_j} - C_{2\epsilon} \rho \frac{\epsilon^2}{k} - R \end{cases} \quad (2)$$

where $\overline{S}_{ij} = \frac{1}{2} \left(\frac{\partial \bar{u}_i}{\partial x_j} + \frac{\partial \bar{u}_j}{\partial x_i} \right)$, $\mu_{\text{eff}} = \mu + \mu_t$, $\mu_t = C_\mu \frac{k^2}{\epsilon}$, and \overline{S}_{ij} are strain rate tensors and R is an additional source term in the ϵ equation representing the influence of average strain rate ϵ . Its expression is

$$R = \frac{C_\mu \eta^3 (1 - \eta / \eta_0) \epsilon^2}{1 + \beta \eta^3} \frac{\epsilon^2}{k}, \eta = Sk / \epsilon \quad (3)$$

The model parameters in the equation above are $C_\mu=0.0845$, $C_{1\epsilon}=1.42$, $C_{2\epsilon}=1.68$, $\alpha_k=1.0$, $\alpha_\epsilon=0.769$, $\beta=0.012$, and $\eta_0=4.38$.

In consideration of viscosity, the non-slip boundary condition was adopted for the wall, and the standard wall function method was used for the area near the wall with a low Reynolds number to deal with the problems caused by the turbulence model with a high Reynolds number. The time discretization of the transient term adopted the first-order implicit format, the spatial discretization of the convection term employed the second-order upwind style, the spatial discretization of the diffusion term utilized the central difference format with second-order precision, and the spatial discretization of the source term used the linear standard format. The coupling of speed and pressure was realized with the SIMPLE algorithm. The under-relaxation factor of all the variables in the iterative calculation was adjusted to 0.1. The time step was 0.0001 s, and the maximum number of iterations was set to 1000 in each time step to ensure absolute convergence in each time step. The convergence residuals of all the solution parameters were 0.0001.

3. DIAGNOSTIC METHOD OF VORTEX DYNAMICS

The obtained internal unsteady flow field should be analyzed to apply the numerical simulation method to the analysis and design of actual fluid machinery problems. The contribution of the local geometry of the impeller to the fluctuation performance at a certain moment was

obtained to provide a basis and guidance for further optimization. The vortex dynamics research method was proposed in the mid-1980s and has been widely adopted since then. The method provides a means to investigate the process of fluid energy increase and the work done by the impeller in the fluid. Compared with the traditional method that uses only velocity and pressure distribution to examine the flow field, the vortex dynamics method is more intuitive and effective. Li et al. used the vortex dynamics method to diagnose the vortex dynamics of a centrifugal pump during the startup process; the method provided a diagnostic basis for impeller design. Vortex dynamics diagnosis of the flow field in a pump is of two main types, namely, diagnosis of the cross section and diagnosis of the boundary vortex flux (BVF). The cross-section diagnosis method is used to examine the process of fluid energy change. The boundary vortex flow diagnosis method is utilized to investigate the work done in the fluid at various local positions on the impeller surface and can provide a direct reference for the design of the pump impeller. The traditional method of flow field analysis analyzes the distribution of velocity and pressure; it is not intuitive, and making fast and accurate judgment is difficult. Meanwhile, the vortex dynamics diagnosis method establishes an objective function in accordance with actual needs. From the perspective of the impeller's work in the fluid, it analyzes the positive or negative contribution of the impeller's local geometric shape on fluid work to provide an intuitive judgment, which plays a guiding role in optimization work.

3.1 Diagnostic method for the cross section

The integral form of the fluid momentum equation is

$$\int_V \rho \frac{Du}{Dt} dV = \int_V \rho f dV + \int_{\partial V} \tau dS \quad (4)$$

where V is the control volume, ρ is density, D/Dt is the satellite derivative, f is the volume force. and τ is the function of spatial variable x , time variable t , and bin direction n , $\tau = \tau(x, t, n)$. This condition shows that a two-rank tensor $T(x, t)$ exists, such that $\tau(x, t, n) = n \cdot T(x, t)$. Then, Equation (4) can be reduced to

$$\rho \frac{Du}{Dt} = \rho f + \Delta \cdot T \quad (5)$$

The dot product of Equation (5) is calculated with velocity vector u in consideration of the symmetry of T . According to the Reynolds transport theorem, the inertial force is much greater than the viscous force at large (Re), which is expressed as follows:

$$\Omega M_z = \frac{\partial K}{\partial t} + G + P + D \quad (6)$$

where ΩM_z is the shaft power applied to the fluid by the impeller. K is the sum of total kinetic energy. and P and D represent the compression and dissipation work of the entire control volume, respectively, expressed as follows:

$$\begin{cases} P = -\int_V p \Delta \cdot u dV \\ D = \mu \int_V \Phi dV \end{cases} \quad (7)$$

where Φ represents the dissipation rate caused by the increase in moisture content. G in Equation (6) represents the energy increase process after the fluid passes through the flow channel, which can be expressed as

$$G = \int_W p^* u_i ds - p_z^* U S_m \quad (8)$$

where W represents the cross section of the flow channel, u_i is the velocity along the streamline direction, U is the axial velocity, S_m represents the inlet section of the flow channel, and p^* and p_z^* are expressed as follows:

$$\begin{cases} p^* = p + \frac{1}{2} \rho |u|^2 \\ p_z^* = p_\infty + \frac{1}{2} \rho |u|^2 \end{cases} \quad (9)$$

where p_∞ represents static pressure, and $P_u = \int_W p^* u_i ds$.

When calculating the shaft power applied by the impeller to the fluid by using Equation (6), for the unsteady flow during the speed fluctuation process, the value of $\partial K / \partial t$ is determined by the acceleration of the speed fluctuation process, the impeller, and the flow channel geometry. The vorticity and expansion of the fluid at the inlet of the passage are small, and the calculated values of P and D in the channel are much smaller than those in P_u . Therefore, P_u is the main parameter in calculating the axial power exerted on the fluid by the impeller blade by using Equation (6), and it is called the total pressure flow. The change objectively reflects the process of fluid energy change in the flow channel and is the main parameter when the flow field is diagnosed by the cross-section method.

3.2 Diagnosis method of BVF

BVF generation rate is a measure of how much vorticity generated per unit area boundary enters the fluid per unit time. It was defined as

$$\sigma = \frac{\mu}{\rho} \frac{\partial \omega}{\partial n} \quad (10)$$

where ω is vorticity, which is defined as $\omega = \nabla \times u$. The dynamic description of σ can be expressed as $\sigma = \sigma_\alpha + \sigma_p + \sigma_\tau$, which refers to the wall acceleration, pressure gradient, and boundary vortex caused by the appendage condition BVF expressed as

$$\begin{cases} \sigma_\alpha = n \times \alpha_B \\ \sigma_p = \frac{1}{\rho} n \times \nabla p \\ \sigma_\tau = \nu (n \times \nabla) \times \omega \end{cases} \quad (11)$$

when the impeller accelerates, the vortex flux σ_α caused by the boundary acceleration and geometric shape of the impeller determine the distribution of blade surface σ_p and σ_τ . Thus, $\rho \sigma_p$ and $\rho \sigma_\tau$ can reflect the effect of impeller acceleration on fluid torque. If Re is large, then σ_τ is much smaller than σ_p and can be ignored. With the z axis as the positive direction, the torque transmitted by the blade to the fluid is determined as follows:

$$M_z = -\frac{1}{2} \int_{S_b} \rho r^2 \sigma_{pz} dS + \frac{1}{2} \int_{S_b} \rho r^2 dz \quad (12)$$

where σ_{pz} is the axial component of boundary vorticity flow σ_p caused by the blade surface pressure gradient, and it can be used for BVF diagnosis.

4. VORTEX DYNAMICS DIAGNOSIS

4.1 Dimensionless analysis

To reveal the transient characteristics of the real-time fluctuation of centrifugal pump speed and eliminate the influence of such speed, we

use dimensionless volume flow and dimensionless head, which are defined as follows:

$$\begin{cases} \phi = Q / \pi D_2 b_2 u_2 \\ \psi = 2gH / u_2^2 \end{cases} \quad (13)$$

where u_2 is the peripheral speed of the impeller outlet, i.e. $u_2 = \pi D_2 n / 60$. Figure 3 shows the time history of the instantaneous dimensionless head and instantaneous dimensionless flow change during the speed fluctuation process and the results calculated based on the quasi-steady state assumption. In the quasi-steady-state calculation, speed was solved using a corresponding similar speed at the same time. If the pump satisfies the quasi-steady-state assumption during the speed fluctuation process, then the results of the transient and quasi-steady-state calculation should be consistent, that is, the instantaneous dimensionless head curve should have a constant value that is independent of speed. The calculation results in Figure 3 show that the instantaneous dimensionless head and instantaneous dimensionless flow exhibited quasi-periodical variation characteristics, which deviated seriously from the prediction characteristics of the quasi-steady state hypothesis, indicating that the quasi-steady state hypothesis cannot be applied to the instantaneous performance prediction of the speed fluctuation process. The change trend of the instantaneous dimensionless head and instantaneous dimensionless flow was completely contrary to the law of speed fluctuation. When the speed reached the maximum value, the instantaneous dimensionless head reached the minimum, but the instantaneous dimensionless flow reached the minimum earlier. Dynamic and static interference had no obvious influence on the instantaneous dimensionless flow; by contrast, they exerted a considerable effect on the instantaneous dimensionless head near high speeds but had minimal influence near low speeds. The law of speed fluctuation in this study was the law of sinusoidal change, and the calculated instantaneous dimensionless flow did not exhibit the law of sinusoidal change.

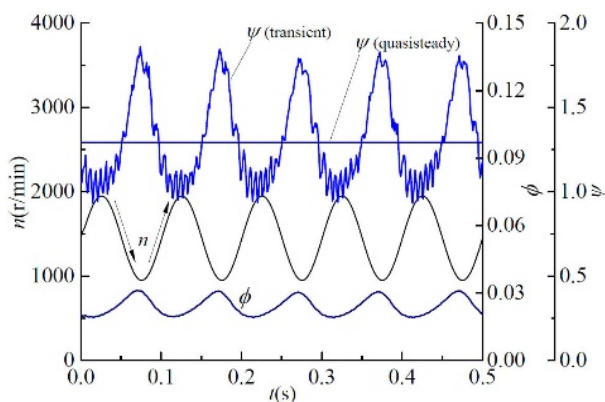


Fig. 3 Temporal course of the change in dimensionless head and dimensionless flow

4.2 Internal flow characteristics

In previous research (Zhao and Zhang (2016)), comparison results of relative streamline evolution based on transient and quasi-steady calculations on the mid-section of the impeller in the deceleration phase during speed fluctuation were initially presented, and the evolution history of transient total pressure was determined based on transient calculation. To determine the complete internal flow characteristics of the model pump during speed fluctuation, this study compared the flow field evolution of the impeller in the acceleration phase (Figure 4) and the quasi-steady-state total pressure evolution derived from quasi-steady-state calculation (Figure 5). The unit of all rotational speed is r/min. The left and right sides of Figure 4 present the relative streamline distributions obtained via transient and quasi-steady-state calculations, respectively. In general, the flow field distribution was complicated, the

internal vortex and secondary flow were obvious, and the vortex area was wide in the quasi-steady-state calculation because flow acceleration inertia was disregarded in such calculation. As the speed increased, the conveying flow increased, and the blade inlet liquid flow and attack angles changed accordingly. Thus, the internal flow field distribution also changed. In the quasi-steady-state calculation, the vortex area was mainly concentrated on the right side of the impeller channel due to the interference of the volute baffle tongue. This result shows that the flow in each impeller channel was not the same, and the flow hydraulic loss in the impeller channel close to the baffle tongue was the largest. Owing to the different flow conditions, the internal pressure presented a non-axisymmetric distribution, which generated a certain radial force.

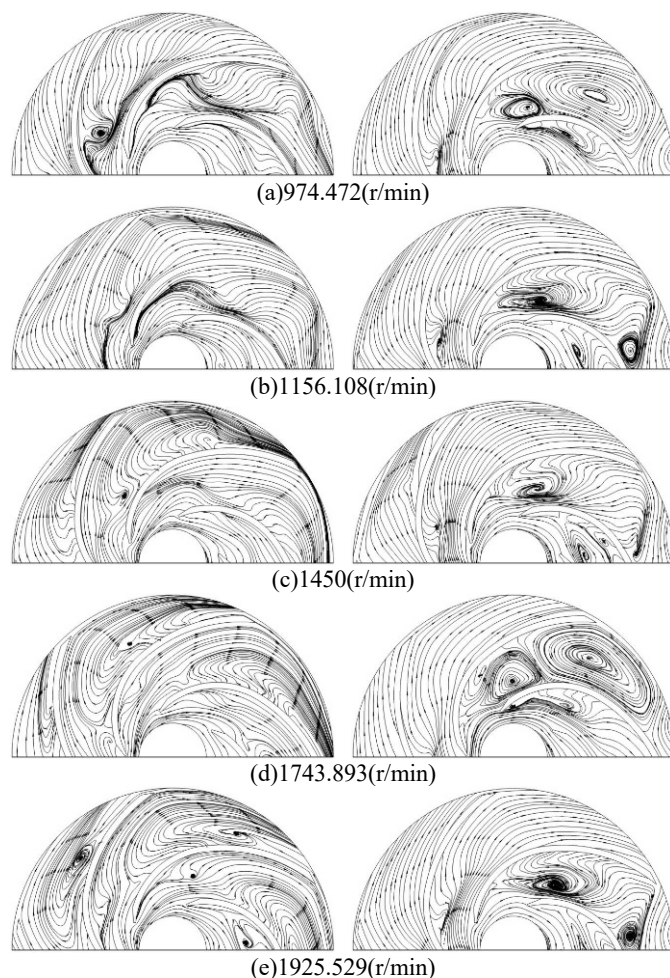


Fig. 4 Evolution characteristics of the impeller flow field in the acceleration stage (left: transient calculation; right: quasi-steady-state calculation)

Figure 5 presents the evolution of total pressure in the acceleration and deceleration phases on the basis of quasi-steady-state calculation. The calculation results showed that the evolution was in line with the general internal flow law of the pump. At any speed, the total pressure on the outer edge of the impeller was much higher than the total pressure on the inner edge; at the same radius, the total pressure of the blade working face was always higher than that of the back. After the fluid flowed out of the impeller and into the volute, the kinetic energy was converted into pressure energy, and the total pressure in the diffuser increased. In the acceleration phase (Figure 5(a)), as the speed increased, the total pressure at the pump outlet increased considerably, whereas the pressure at the center of the impeller decreased. The maximum speed was 1950 r/min, which is not too high. Numerical simulation showed that the lowest absolute pressure at the center was 100 kPa, which is much higher than the vaporization pressure of 2367.8 Pa.

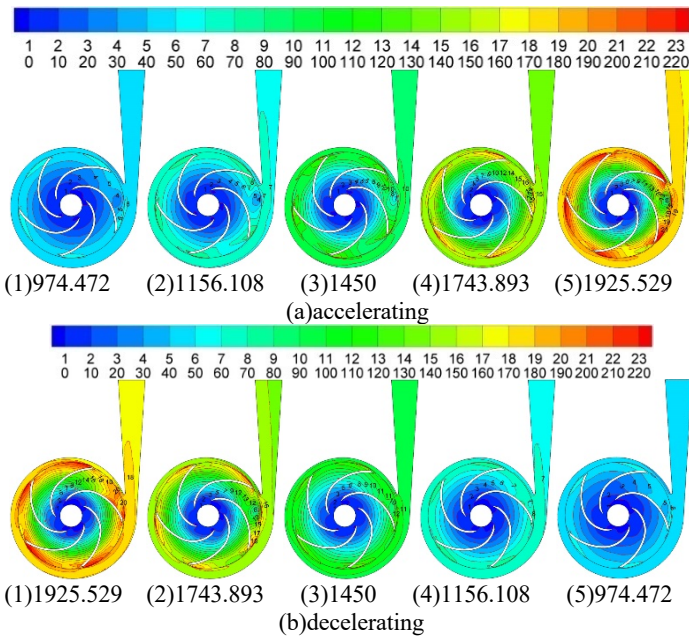


Fig. 5 Quasi-steady-state total pressure distribution (kPa)

4.3 Diagnosis of total pressure flow in the cross section

In the impeller passage, a series of flow sections perpendicular to the radius were created from the inlet side to the outlet side of the impeller along the cross-flow direction, and the total pressure flow integral was established for each section. The change curve of the value at different radii in the stage of speed decrease and increase is shown in Figure 6. At different rotation speeds, the fluid energy gradually increased along the flow direction in the impeller, which fully reflected the work effect of the impeller on the fluid and was consistent with the flow theory in the pump. When the speed decreased, the speed value continued to decrease with the passage of time in the fluctuating process, and the curve decreased as a whole. This result indicates that the fluid energy continued to decrease, thus reflecting the true work process. When the speed increased, the flow conversion situation was the complete opposite, and the total pressure flow energy continued to rise. Given that the acceleration values are equal and contrasting in the phases of speed decrease and increase, respectively, this condition is expected to cause differences in the flow distribution of the two phases.

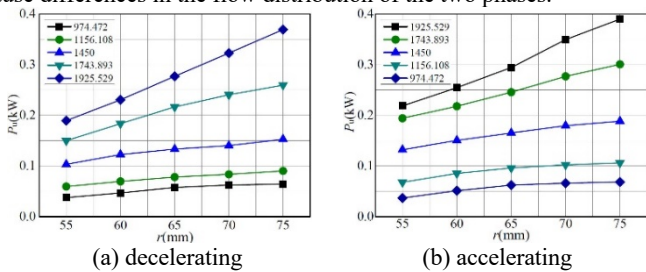


Fig. 6 Distribution of the total pressure flow integral along the radius in different stages

Figure 7 shows a comparison of the total pressure flow integral. The fluid energy when the speed was reduced was generally larger than the value when the speed increased, indicating that the hydraulic losses in the two phases differed. When the speed increased, pressure energy was converted into kinetic energy, and the speed value increased continuously. The hydraulic loss was relatively large at this stage because such loss is proportional to the square of speed. The fluid energy value was thus low. When the speed decreased, kinetic energy was converted into pressure energy, the speed value decreased continuously, and the hydraulic loss was small; hence, the energy value was high. However, when the speed value was 974.472 r/min, the fluid energy value in the acceleration phase was greater than that in the

deceleration phase near the impeller inlet. This result is related to the reduced speed phase value. Although the flow speed and flow loss continued to increase when the speed increased, the value was relatively small. Thus, the energy at the inlet was high.

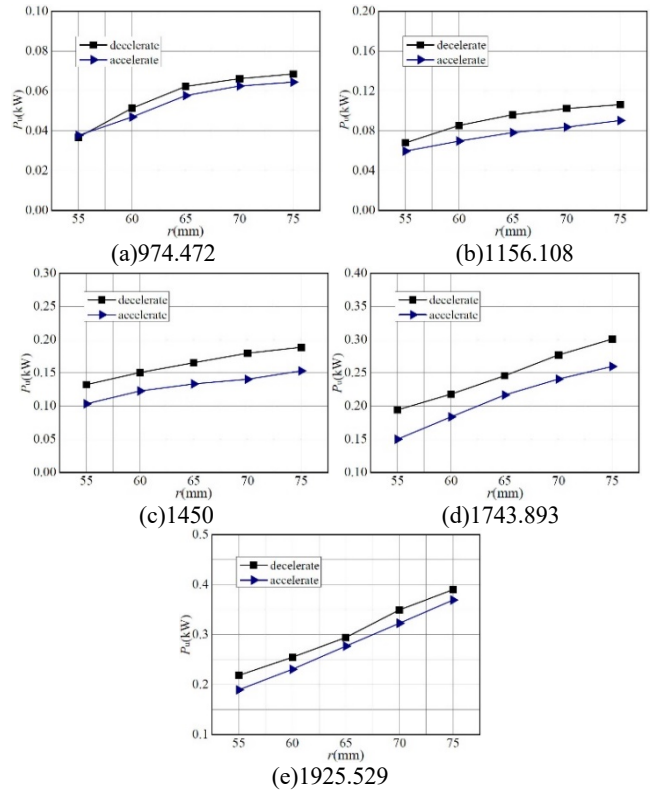


Fig. 7 Comparison of the total pressure flow integral at the same speed in different stages

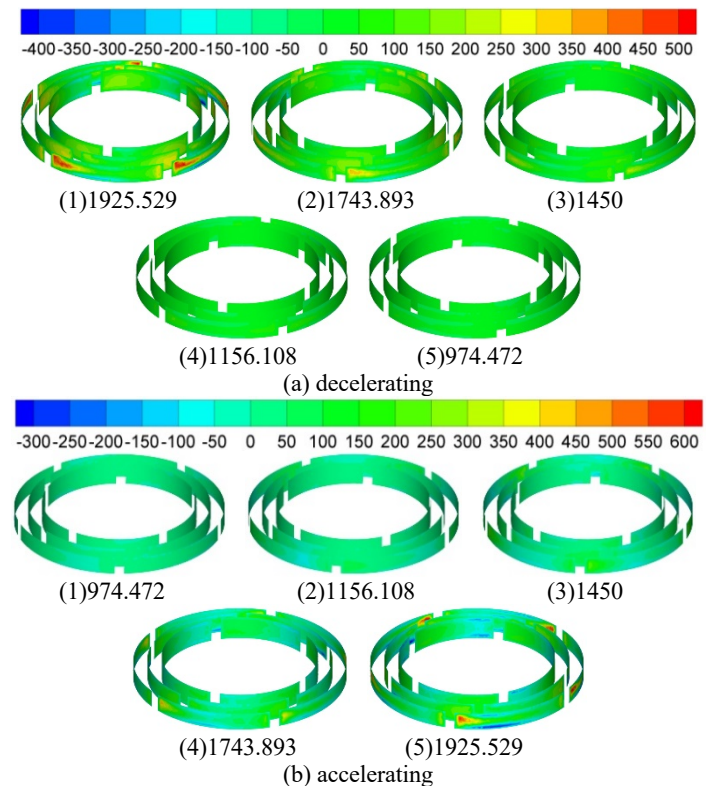


Fig. 8 Distribution of total pressure flow at different radii of the cross section (from inside to outside: $r = 0.055, 0.065, 0.075$ m)

Figure 8 shows the detailed evolution of the total pressure flow distribution in each section during the deceleration and acceleration stages. In general, the total pressure flow distribution in the middle of the impeller was uniform, energy unevenness occurred locally in the cross section near the inlet and outlet positions. The dynamic and static interference effect caused by the baffle tongue structure was the source of the uneven energy.

4.4 Diagnosis of BVF on the blade surface

The axial component of σ_p , σ_{pz} reflects the magnitude of the effective torque applied by the impeller to the fluid in the direction of z and can be used as an important reference index for the diagnosis of BVF distribution on the blade surface. BVF is the source of vortex flux in the flow field and can be adopted as a criterion for analyzing and judging blade design.

A positive BVF distribution provides a negative contribution, and a negative BVF distribution provides a positive contribution. Therefore, the positive BVF distribution area should be eliminated as much as possible during blade design, that is, the area of negative contribution to fluid work should be minimized. The calculation results in Figure 9 suggest that at different speeds during the speed fluctuation process, a large positive BVF distribution was observed in the upper part of the blade, especially on the pressure surface side, indicating that the work done by this part provided a negative contribution to the fluid and that the region should be eliminated. CFD technology can be used to predict this situation in the design and provide a basis for modification. When designing the impeller, the BVF distribution should be as uniform as possible to reduce the peak value of BVF, and the BVF area with a negative contribution should be eliminated as much as possible.

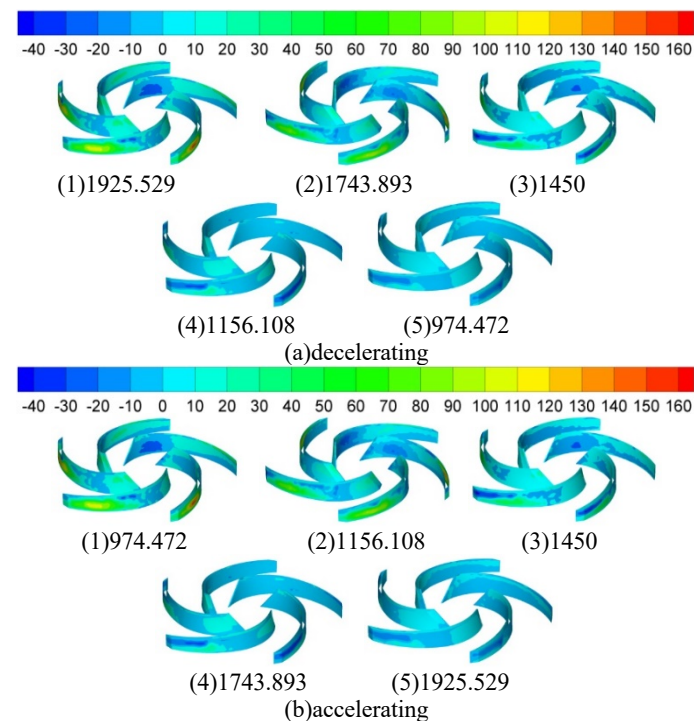


Fig. 9 Distribution and evolution of BVF on the blade surface at different stages

5. CONCLUSION

The diagnosis results of the flow section showed that the total pressure flow gradually increased along the direction of the flow channel during the process of speed fluctuation, indicating that the impeller was providing functional power. When the speed decreased, the total pressure flow gradually decreased; when the speed increased, the total pressure flow gradually increased. The influence of the conversion of

kinetic and pressure energy in the deceleration and acceleration stages made the total pressure flow energy different. During the deceleration process, the hydraulic loss was small, and the total pressure flow energy was high. On the contrary, the total pressure flow energy was low in the acceleration stage. Through CFD and boundary vorticity current diagnosis methods, the BVF distribution is made as uniform as possible, and the designer can obtain a basis for quickly modifying the blade profile, thereby serving practical applications.

During speed fluctuation, the change rules of the instantaneous dimensionless head and instantaneous dimensionless flow were completely contradictory to that of speed fluctuation; instantaneous dimensionless flow did not exhibit sinusoidal fluctuation. Compared with the internal flow field from the transient calculation, that obtained by the quasi-steady calculation was more complicated. These results indicate that the quasi-steady-state assumption cannot be applied to instantaneous performance prediction in the process of speed fluctuation. The baffle tongue plays an important role in the hydraulic loss and radial force distribution in the impeller and thus requires further attention and investigation.

ACKNOWLEDGEMENTS

The research was financially supported by the “Pioneer” and “Leading Goose” R&D Program of Zhejiang (Grant No. 2022C03170), Science and Technology Project of Quzhou (Grant No.2022K98), National Natural Science Foundation of China (Grant No. 51876103), and Zhejiang Provincial Natural Science Foundation of China (Grant No. LZY21E060001 and LZY21E060002).

REFERENCES

- Abed, I.M., Ali, H.F., and Sahib, S.A.M., 2020, “Investigation of heat transfer and fluid flow around sinusoidal corrugated circular cylinder for two-dimensional system,” *Frontiers in Heat and Mass Transfer*, **15**(6), 1–9.
<http://dx.doi.org/10.5098/hmt.15.6>
- Dai, J., Liu, X.Q., and Huang, C.B., 2021, “Experiment on Pressure Pulsation of Axial Flow Pump System with Different Runaway Head,” *Processes*, **9**(9), 1597–1608.
<https://doi.org/10.3390/pr9091597>
- Dazin, A., Caignaert, G., and Bois, G., 2007, “Transient behavior of turbomachineries: applications to radial flow pump startups,” *Journal of Fluid Engineering*, **129**(11), 1436–1444.
<https://doi.org/10.1115/1.2776963>
- Duplaa, S., Coutier-Delgosha, O., and Dazin, O., 2010, “Experimental study of a cavitating centrifugal pump during fast startups,” *Journal of Fluid Engineering*, **132**(2), 1–12.
<https://doi.org/10.1115/1.4000845>
- Gu, X.Y., Jiang, G.H., and Wo, Y., 2020, “Numerical study on heat transfer characteristics of propylene glycol-water mixture in shell side of spiral wound heat exchanger,” *Frontiers in Heat and Mass Transfer*, **15**(3), 1–8.
<http://dx.doi.org/10.5098/hmt.15.3>
- Lefebvre, P.J., and Barker, W.P., 1995, “Centrifugal pump performance during transient operation,” *Journal of Fluid Engineering*, **117**(1), 123–128.
<https://doi.org/10.1115/1.2816801>
- Li, Z.F., Wu, D.Z., and Wang, L.Q., 2010, “Numerical simulation of the transient flow in a centrifugal pump during starting period,” *Journal of Fluids Engineering*, **132**(8), 1–8.
<https://doi.org/10.1115/1.4002056>

- Liu, J.T., Li, Z.F., and Wang, L.Q., 2011, "Numerical simulation of the transient flow in radial flow pump during stopping period," *Journal of Fluids Engineering*, **133**(11), 1-7.
<https://doi.org/10.1115/1.4005137>
- Tanaka, T., and Tsukamoto, H., 1999, "Transient behavior of a cavitation centrifugal pump at rapid change in operating conditions-Part 1: Transient phenomena at opening/closure of discharge valve," *Journal of Fluid Engineering*, **121**(4), 841-849.
<https://doi.org/10.1115/1.2823545>
- Tanaka, T., and Tsukamoto, H., 1999, "Transient behavior of a cavitation centrifugal pump at rapid change in operating conditions-Part 2: Transient phenomena at pump startup/shutdown," *Journal of Fluid Engineering*, **121**(4), 850-856.
<https://doi.org/10.1115/1.2823546>
- Tsukamoto, H., Matsunaga, S., and Yoneda, H., 1986, "Transient characteristics of a centrifugal pump during stopping period," *Journal of Fluids Engineering*, **108**(4), 392-399.
<https://doi.org/10.1115/1.3242594>
- Tsukamoto, H., and Ohashi, H., 1982, "Transient characteristics of a centrifugal pump during startup period," *Journal of Fluids Engineering*, **104**(1), 6-13.
<https://doi.org/10.1115/1.3240859>
- Tsukamoto, H., Yoneda, H., and Sagara, K., 1995, "The response of a centrifugal pump to fluctuating rotational speed," *Journal of Fluids Engineering*, **117**(3), 479-484.
<https://doi.org/10.1115/1.2817287>
- Wu, D.Z., Wu, P., and Li, Z.F., 2010, "The Transient Flow in a Centrifugal Pump during the Discharge Valve Rapid Opening Process," *Nuclear Engineering and Design*, **240**(12), 4061-4068.
<https://doi.org/10.1016/j.nucengdes.2010.08.024>
- Wu, D.Z., Wu, P., and Yang, S., 2014, "Transient characteristics of a close-loop pipe system during pump stopping periods," *Journal of Pressure Vessel Technology*, **136**(2), 1-8.
<https://doi.org/10.1115/1.4025616>
- Xue, R., Lin, X.Y., and Zhang, B.L., 2022, "CFD and Energy Loss Model Analysis of High-Speed Centrifugal Pump with Low Specific Speed," *Applied Sciences*, **12**(15), 7435-7447.
<https://doi.org/10.3390/app12157435>
- Yakhot, V., and Orzag, S. A., 1986, "Renormalization group analysis of turbulence: basic theory," *Journal of Scientific Computing*, **1**(1), 3-51.
<https://doi.org/10.1007/BF01061452>
- Zhang, Y.L., Xiao, J.J., and Zhao, Y.J., 2014, "Numerical investigation on a prototype centrifugal pump subjected to fluctuating rotational speed," *Mathematical Problems in Engineering*, 436473.1-8.
<https://doi.org/10.1155/2014/436473>
- Zhang, Y.L., Zhu, Z.C., and Li, W.G., 2019, "Non-inertial stopping characteristics of a prototype pump," *Advances in Mechanical Engineering*, **11**(4), 1-15.
<https://doi.org/10.1177/1687814019844649>
- Zhao, Y.J., and Zhang, Y.L., 2016, "Study of the Transient Response Characteristics of a Centrifugal Pump Undergoing a Drastic Fluctuation in the Rotating Speed," *Journal of Engineering for Thermal Energy & Power*, **31**(5), 106-112. (in Chinese with English abstract)
<https://doi.org/10.16146/j.cnki.rndlgc.2016.05.016>